PERGAMON

Journal of Geodynamics 31 (2001) 557–576

JOURNAL OF
GEODYNAMICS

www.elsevier.com/locate/jgeodyn

Centrifuge models simulating magma emplacement during oblique rifting

Giacomo Corti[a,*], Marco Bonini[b], Fabrizio Innocenti[a], Piero Manetti[c], Genene Mulugeta[d]

[a]*Dipartimento di Scienze della Terra, Università degli Studi di Pisa, via S. Maria, 53, 56126 Pisa, Italy*
[b]*Analogue Modelling Laboratory, CNR, Centro Studio Geologia dell'Appennino e delle Catene Perimediterranee, via La Pira, 4, 50121 Firenze, Italy*
[c]*Dipartimento di Scienze della Terra, Università degli Studi di Firenze, via La Pira, 4, 50121 Firenze, Italy*
[d]*Hans Ramberg Tectonic Laboratory, Institute of Earth Sciences, Uppsala University, Villavagen 16, 752 36 Uppsala, Sweden*

Received 8 December 2000; accepted 21 May 2001

Abstract

A series of centrifuge analogue experiments have been performed to model the mechanics of continental oblique extension (in the range of 0° to 60°) in the presence of underplated magma at the base of the continental crust. The experiments reproduced the main characteristics of oblique rifting, such as (1) en-echelon arrangement of structures, (2) mean fault trends oblique to the extension vector, (3) strain partitioning between different sets of faults and (4) fault dips higher than in purely normal faults (e.g. Tron, V., Brun, J.-P., 1991. Experiments on oblique rifting in brittle-ductile systems. Tectonophysics 188, 71–84). The model results show that the pattern of deformation is strongly controlled by the angle of obliquity (α), which determines the ratio between the shearing and stretching components of movement. For $\alpha \leqslant 35°$, the deformation is partitioned between oblique-slip and normal faults, whereas for $\alpha \geqslant 45°$ a strain partitioning arises between oblique-slip and strike-slip faults. The experimental results show that for $\alpha \leqslant 35°$, there is a strong coupling between deformation and the underplated magma: the presence of magma determines a strain localisation and a reduced strain partitioning; deformation, in turn, focuses magma emplacement. Magmatic chambers form in the core of lower crust domes with an oblique trend to the initial magma reservoir and, in some cases, an en-echelon arrangement. Typically, intrusions show an elongated shape with a high length/width ratio. In nature, this pattern is expected to result in magmatic and volcanic belts oblique to the rift axis and arranged en-echelon, in agreement with some selected natural examples of continental rifts (i.e. Main Ethiopian Rift) and oceanic ridges (i.e. Mohns and Reykjanes Ridges).

* Corresponding author. Fax: +39-050-500932.
E-mail address: corti@dst.unipi.it (G. Corti).

0264-3707/01/$ - see front matter
PII: S0264-3707(01)00032-1

1. Introduction

During oblique rifting the deformed zone trends obliquely to the stretching vector, such that both extension perpendicular to the rift trend and shear parallel to the rift trend contribute to rift formation (e.g. Withjack and Jamison, 1986). Such an oblique extension can arise because of: (1) reactivation of pre-existing crustal zone of weakness trending oblique to the stretching vector, or (2) rotation of the direction of extension through time (e.g. Bonini et al., 1997; Clifton et al., 2000). In both cases, the ratio between the shearing and stretching component, and hence the resulting structural pattern, depends on the angle between the extension vector and the rift trend (i.e. angle of obliquity, α).

Previous scaled analogue models have been successfully applied to the analysis of the deformation pattern resulting from oblique extension (Withjack and Jamison, 1986; Tron and Brun, 1991; Brun and Tron, 1993; Dauteuil and Brun, 1993, 1996; McClay and White, 1995; Scott and Benes, 1996; Bonini et al., 1997; Mart and Dauteuil, 2000; Clifton et al., 2000). In particular, these models have reproduced the main structural characteristics of oblique rifting, such as (1) en-echelon faults with a component of displacement varying from pure normal to strike-slip; (2) mean fault trends oblique to the extension vector; (3) strain partitioning between different sets of structures and (4) fault dips generally steeper than in pure normal faults (e.g. Tron and Brun, 1991).

In this paper we explore, through the use of scaled centrifuge models, the effects of magma underplating the continental crust on the structural pattern resulting from oblique rifting. In particular, we analyse the upper and lower crust deformation and the characteristics of magma emplacement, focussing on the dynamic interactions between these two processes; then we compare model results with natural examples of continental and oceanic oblique rifting.

2. Analogue modelling

2.1. Experimental procedure

A series of 10 small-scale experiments has been performed at the Hans Ramberg Tectonic Laboratory, Uppsala University (Sweden) to investigate the relationships between structural evolution and magma emplacement in the continental crust during oblique rifting. All models were deformed in an artificial gravity field of 200 g by using a centrifugal apparatus (Ramberg, 1981). The models were built in an aluminum box with dimension $6.6\times6.5\times12$ cm, surrounded by plasticine placed inside a wider Plexiglas box of dimension $19\times19\times15$ cm (Fig. 1). The aluminum box was divided into two halves, one of which was allowed to move during successive runs in the centrifuge (Fig. 1). The other half was stationary. A thin acetate sheet was fixed to the base of moving part of the aluminum box, allowing half of the model to move solidly with the box. This set-up created a velocity discontinuity (VD) in the central part of the model, parallel to the main rift trend (e.g. Allemand et al., 1989; Tron and Brun, 1991). The VD also coincided with the trend of the magma initially underplated at the base of the crust (see later; Fig. 1). To minimise boundary friction, the bottom and the side walls of the moving half of the box were lubricated either with liquid soap or vaseline.

Oblique rifting was obtained and controlled by removing slices of plasticine at two extremities of the moving half of the model during successive runs in the centrifuge (Fig. 1). In response to

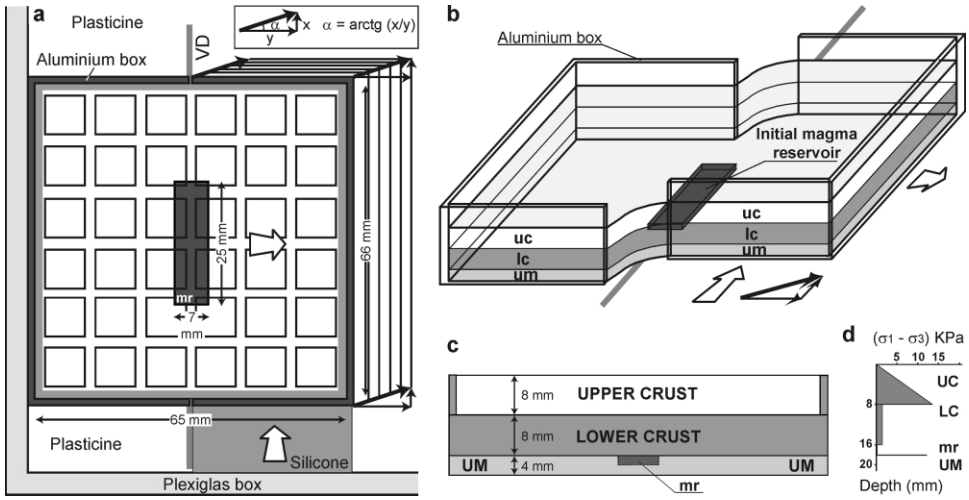

Fig. 1. Initial model set-up, arrangement and initial strength profile. UC: upper crust; LC: lower crust; UM: upper mantle; mr: magma reservoir; VD: velocity discontinuity.

the centrifugal body force field, vertical collapse and lateral expansion of the model took place in a direction perpendicular to the VD (Fig. 1). This movement was partly accompanied by the lateral expansion of a piece of silicone putty at one end of the aluminum box, which generated a vector parallel to the VD (Fig. 1). The sum of the two vectors resulted in a mean displacement vector oblique to the central VD with an obliquity angle (α) mainly controlled by the amount of plasticine removed (Fig.1). This angle was varied during the experiments from 0° to about 60° (see Table 1); in all models, the displacement along the central VD was left-lateral. Four models (ObR2, 3, 4, 5bis and 9) were performed in the presence of a squared magma chamber with dimension of 2.5 cm×0.7 cm×0.2 mm, placed at the base of the model continental crust (Fig. 1, Table. 1). To compare results, corresponding models (ObR 6, 7, 8 and 10) were also performed without introducing the magma chambers (see Table 1).

All the models were allowed to stretch laterally at 30 s intervals in order to control the velocity of stretching and the amount of extension (see Table 1). To compare model results, these two factors (velocity and bulk extension) were kept constant in all models (see Table 1). Top-view photos of the models were taken at various stages. After a successful experiment, the models were frozen before taking a number of cross-sections to study their 3D internal geometry.

2.2. Analogue materials

The simplified strength profiles of the continental lithosphere can be approximated by using dynamically scaled brittle and ductile layers. Previous analogue studies have demonstrated that these two end-member deformation mechanisms can be successfully modelled in laboratory using sand to represent brittle layers and silicone putty to simulate the ductile layers (see Brun, 1999, for a review).

We investigated the deformation of the continental crust in a two-layer brittle–ductile system by simplifying the initial rheological conditions in natural rifts assuming a basaltic magma underplated

Table 1
Parameters of models deformation

Model	Obliquity angle (α)	$\beta_{(vector)}$	Initial magma chamber dimensions	Average velocity of extension (mm/s)
ObR2	13°	1.43	2.5×0.7 cm	$2.2\ 10^{-1}$
ObR3	35°	1.42	2.5×0.7 cm	$1.3\ 10^{-1}$
ObR4	46°	1.56	2.5×0.7 cm	$1.8\ 10^{-1}$
ObR5	57°	1.48	2.5×0.7 cm	$1.3\ 10^{-1}$
ObR6	45°	1.58	No magma	$1.7\ 10^{-1}$
ObR7	30°	1.56	No magma	$2.6\ 10^{-1}$
ObR8	20°	1.45	No magma	$1.6\ 10^{-1}$
ObR9	0°	1.36	2.5×0.7 cm	$1.0\ 10^{-1}$
ObR10	0°	1.36	No magma	$1.1\ 10^{-1}$

at the base of the crust (e.g. Furlong and Fountain, 1986; Bergantz, 1989; Fyfe, 1992; Parsons et al., 1992) and a brittle/ductile ratio of about 1, implying that these conditions simulated a relatively advanced rifting stage (e.g. Fadaie and Ranalli, 1990).

The upper continental crust was simulated using a layer of sand (8 mm thick) with a density of $\rho_b \approx 1300$ kg m^{-3} and an angle of internal friction of $\Phi \approx 30°$. To avoid its collapse when introducing the models vertically in the centrifuge apparatus, sand was wetted with paraffin oil to make it more cohesive without thereby violating dynamic similitude (see Mulugeta, 1988). The underlying lower crust was simulated by an 8 mm thick mixture of Rhodosil Gomme 70009 (manufactured by Rhone Poulenc, France) and dry quartz-sand. This mixture exhibited a near-Newtonian behaviour at the employed experimental strain rates of $\approx 10^{-2}$ s^{-1}, with a dynamic viscosity of $\eta = 6\ 10^4$ Pa s. The density of this layer was $\rho_d \approx 1490$ kg/m^3.

The upper part of the lithospheric mantle was simulated using a 4 mm layer of a denser sand-silicone mixture ($\rho_m \approx 1560$ kg m^{-3}) with an effective viscosity of $\eta_m \approx 10^5$ Pa at the experimental strain rate.

Magma was reproduced in the experiments by using glycerol, a low-viscosity (1 Pa s) Newtonian material with a density of $\rho_v = 1260$ kg m^{-3}. This material was mixed with a red pigment to enhance the colour contrast.

2.3. Scaling and model ratios

The experiments have been scaled following the principles of similitude outlined by Hubbert (1937) and Ramberg (1981). We have assumed an initial thickness of the crust of about 30 km and a brittle/ductile crust thickness ratio of about 1, such that the model to nature ratio of length l^* is 5.3×10^{-7}. Models can be scaled down to nature starting from the equation

$$\sigma^* = \varepsilon^* \eta^* \tag{1}$$

where σ^*, η^*, ε^*, are the stress, viscosity and strain-rate model to nature ratios.

The model/nature ratios of density ($\rho^* \approx 0.5$) and gravity ($g^* = g_m/g_n = 200$) imposes a ratio of normal stress of $\sigma^* = \rho^* g^* l^* = 5.3\times10^{-5}$. Viscosity ratio η^* ranges from 6×10^{-16} up to 6×10^{-20},

considering $\eta_m = 6\ 10^4$ Pa s and prototype viscosity values η_n of the lower continental crust in the range 10^{20} to 10^{24} Pa s (e.g. Buck, 1991; Weijermars, 1997). From Eq. (1), one can obtain $\varepsilon^* = \sigma^*/\eta^*$ (e.g. Merle and Vendeville, 1995), such that ε^* ranges from 8.8×10^{10} to 8.8×10^{14}. Following Merle and Abidi (1995), the horizontal displacement rate $v^* = v_m/v_n$ is given by the product of ε^* and l^*, such that an average viscosity of 10^{21} Pa s corresponds to $v_n \sim 13$ mm year^{-1}, that may represent an average extension rate for continental rift systems (e.g. 3 to 22 mm year^{-1} in the Main Ethiopian Rift–Afar system; Hayward and Ebinger, 1996).

2.4. Limitations of models

The main limitation of our centrifuge models is related to the simplified rheological layering, that implicitly assume thermal equilibrium during deformation. In nature, instead, rheological and thermal variations in the continental crust and in magmas characterise the rifting process (e.g. Buck, 1991).

Another limitation concerns that pre-existing fabrics within the upper crust, reactivated during oblique rifting, are not suitably accounted in current analogue experiments (Morley, 1999a). However, in natural oblique rift systems involving an underplated magma, the main anisotropy is expected to occur at the base of the crust, as a consequence of both thermal weakening of the crust and strain localisation caused by the presence of magma (e.g. Arzi, 1978; Chèry et al., 1989; Morley, 1999b).

Another consequence of the model set-up involving the occurrence of a basal central VD, is that the latter will affect the local stress orientation in a dominant way (Morley, 1999a). However, during our experiments extension occurred mainly because of a gravitational collapse of the ductile layers and not because of the pulling apart of a metal or plastic sheets at the base of the models (e.g. Withjack and Jamison, 1986; Tron and Brun, 1991). Furthermore, the stress perturbation imposed by the VD is redistributed in the whole crust through the upper mantle, such that the presence of the thin acetate sheet has only a minor influence on the model deformation pattern.

However, we consider the above limitations of minor importance with respect to the process under investigation; therefore the analogue experiments are relevant for the comprehension of the relationships between deformation and magma emplacement during oblique rifting.

3. Experimental results

The dynamics of magma emplacement during oblique rifting was investigated by considering increasing angles of obliquity (from 0° to about 60°) for a given brittle/ductile crust thickness ratio and a given strain rate. All models showed two main types of deformation (Fig. 2): faulting in the brittle sand layer and ductile flow in the silicone layer. Faulting in the upper crust resulted in the development of normal to oblique-slip en-echelon faults bounding crustal-scale grabens which formed in the central area of the models (Figs. 2 and 3). The component of lateral displacement of the border faults increased with increasing the angle α, whereas for high obliquity angles (i.e. $\alpha \geq 45°$) discrete strike-slip faults were observed beside the major grabens.

Ductile flow resulted in the development of lower crust domes that typically rose and warped-up the brittle/ductile interface. These domes were characterised by an elongated shape that followed,

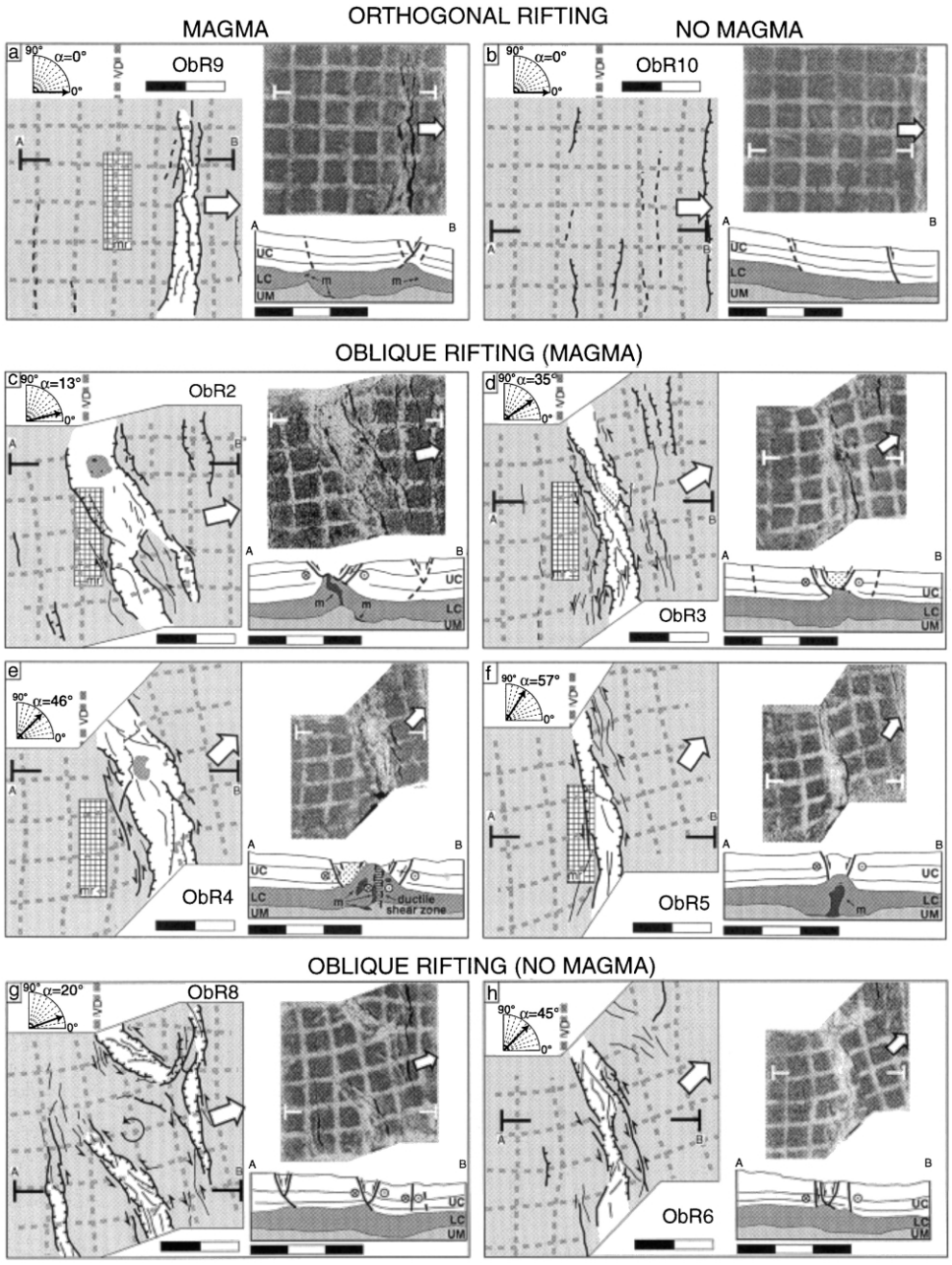

Fig. 2. Top-view line drawings, top views and cross-sections of oblique and orthogonal rifting models. (a) Orthogonal rifting model with magma and (b) orthogonal rifting model without magma; (c–f) oblique rifting models with magma at the base of the crust; (g–h) oblique rifting models without magma. The initial position of the magma reservoir (mr) and the velocity discontinuity (VD) are indicated; arrows point the displacement vector direction. The trace of the cross-sections is indicated in black in the line drawing and white on the model top-surface. Stippled pattern indicate magma intrusions in the model upper crust. The scale bars are in cm.

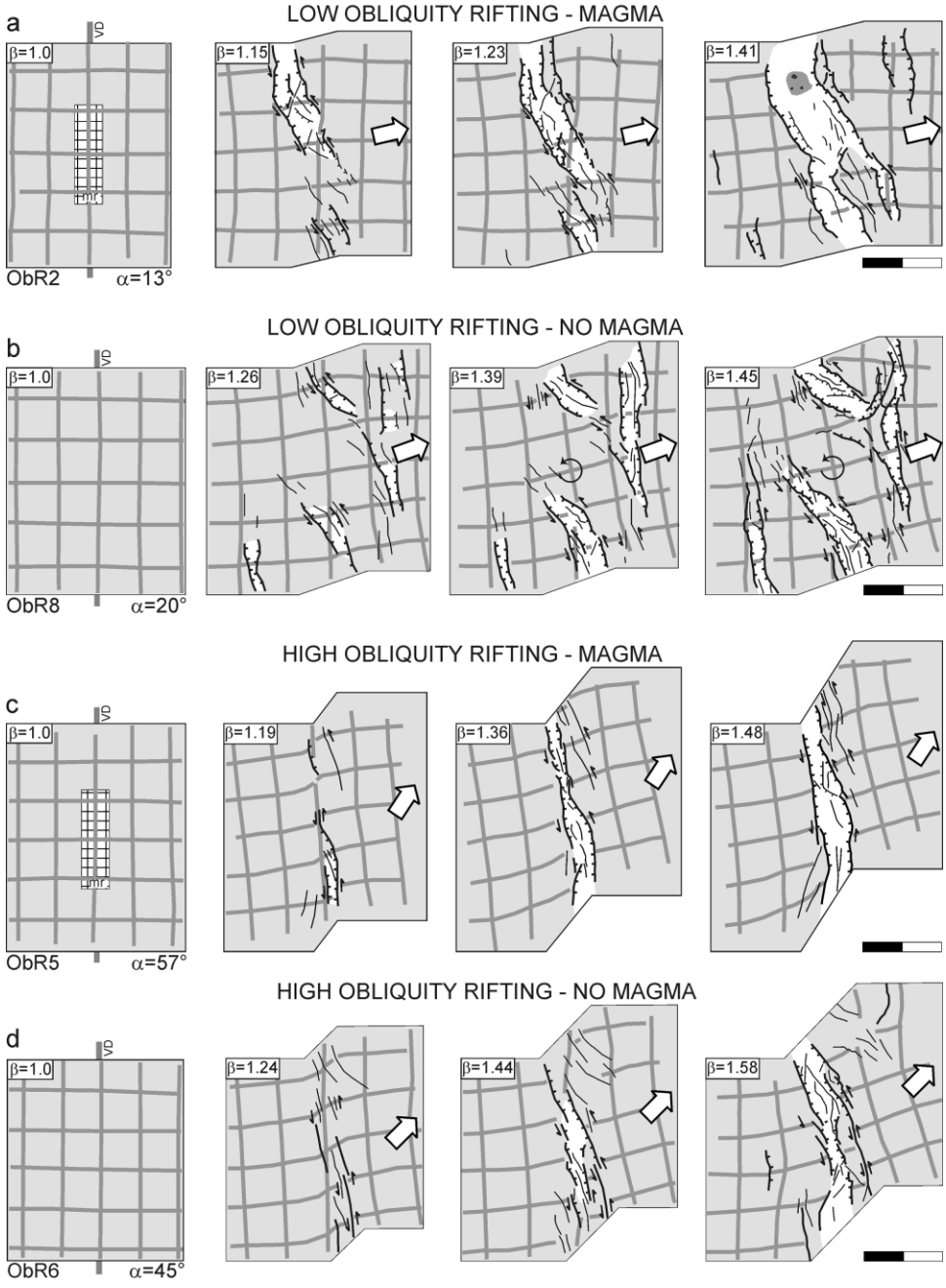

Fig. 3. Sequential top view line drawings of the main steps during deformation of models ObR2 (a), ObR8 (b), ObR5 (c) and ObR6 (d). The initial position of the magma reservoir (mr) and the velocity discontinuity (VD) are indicated. The scale bars are in cm.

at depth, the trend of the overlying grabens. Typically, magma emplaced at the core of these lower crustal domes, which represents a zone of relatively low pressure (Fig. 2).

3.1. Surface fault pattern—low obliquity rifting ($\alpha \leqslant 35^\circ$)

For low obliquity rifting ($\alpha \leqslant 35^\circ$; models ObR2, 3, 7 and 8) the surface fault pattern was characterised by the development of different sets of faults trending parallel and oblique to the central VD (Fig. 2c, d and g). Faults parallel to the VD formed toward the edges of the models and showed an almost pure-normal component of movement, whereas VD-oblique faults affected the central part of the model and showed an oblique-slip component of displacement. Oblique faults were typically arranged en-echelon and characterised by a markedly tortuous fault trace (Fig. 2c; d).

In models with underplated magma (ObR2 and ObR3, Fig. 2c and d), deformation was mainly accommodated by slip along the central oblique faults defining a prominent central graben. During the initial stages of rifting two grabens, typically bordered by en-echelon normal to oblique-slip faults, formed at the lateral edges of the models (Fig. 3a, $\beta = 1.15$). For increasing extension, they joined into a central graben that widened progressively whereas external normal faults formed only in the latest stages of model deformation (Fig. 3a, $\beta = 1.41$). Notably, some oblique dextral faults developed to accommodate the rotation of fault-bounded internal blocks (e.g. McKenzie and Jackson, 1983, 1986; Fig. 2c). Statistical analysis of fault distribution show that oblique faults have an orientation that corresponds to the main peak in the length-weighted histograms, whereas external normal faults are expressed by the VD-parallel secondary peak (Fig. 4a and b).

In experiments without magma at the base of the crust (ObR7 and ObR8; Figs. 2g, 3b and 5d), the central part of the model was characterised by the development of two en-echelon grabens, which formed near the two extremities of the aluminium box simultaneously with external normal faults (Fig. 3b). In contrast to the models with magma, these grabens never joined together and the central portion of the models was partially undeformed and was subjected to a counterclockwise block rotation, as documented by the deformation of the initial grid (Fig. 5c and d). The final fault pattern was more complex than in models with magma at the base as documented by the polymodal frequency distribution in the histogram of fault orientation (Fig. 4f and g).

=45¤)",5,0,2,0,309pt,309pt,0pc,0pc>3.2. Surface fault pattern—high obliquity rifting ($\alpha \geqslant 45^\circ$)

For high obliquity rifting ($\alpha \geqslant 45^\circ$; models ObR4-6), upper crust deformation was partitioned between normal to oblique-slip faults, bounding narrow central grabens, and strike-slip faults (Fig. 2e, f and h). In the lower crust the increased strike-slip component of movement was accommodated by the development of rift-parallel ductile shear zones which formed within the ductile domes (Fig. 2e and f). The progressive deformation of model ObR5 shows that the en-echelon oblique faults formed in the earliest stages of rifting, almost simultaneously with external discrete strike-slip structures (Fig. 3c; $\beta = 1.19$). With increasing extension, the oblique en-echelon faults joined together giving rise to a narrow graben that widened progressively contemporaneously with the development of other strike-slip structures (Fig. 3c; $\beta = 1.48$). Notably, in response to the increase of the shearing component, the fault dip was higher than in low obliquity rifting and the

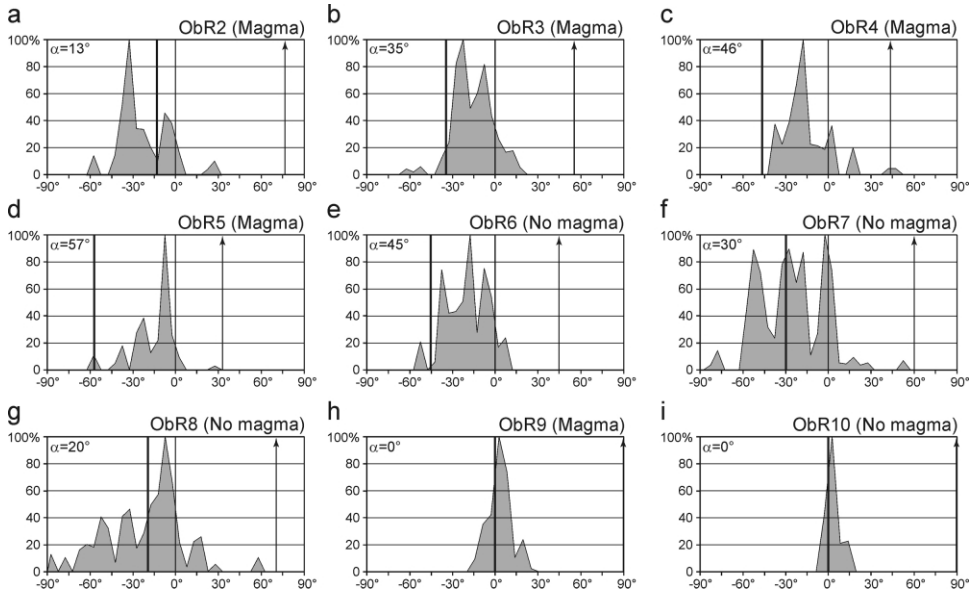

Fig. 4. Statistical analysis of fault orientation for models ObR2-10. The orientation of faults is measured considering the VD as the reference line; positive and negative angles correspond to clockwise and couterclockwise measurements, respectively. On histograms frequencies have been weighted according to fault length such that values in the graphs represent, for intervals of 5° of orientation, the sum of the length of fault segments which have the considered orientation, normalised to the maximum value. Only the faults present in the central part of the model have been taken into account for the statistical analysis. The black arrow indicate the stretching direction, the thick line is orthogonal to the extension direction, and the thin line is parallel to the VD.

width of deformed zone (here calculated for models ObR2-8 and for $\beta = 1.4$) decreased with an abrupt change at α between 35° and 45° (Fig. 2e and f; Fig. 6).

During high obliquity rifting experiments, no marked differences have been observed between models with magma (ObR4 and 5; Figs. 2e and f and 3c) and models without magma at the base of the crust (ObR6, Figs. 2h and 3d). In both cases, the analysis of fault orientation shows that the majority of faults are oblique or slightly oblique to the deformed zone, although secondary VD-parallel peaks in the fault distribution histogram also occur (Fig. 4c–e). These peaks are related to straight fault segments lying directly above the VD (e.g. Tron and Brun, 1991; Fig. 2e and h).

3.3. Lower crust doming

Cross sections and photographs of the top of the ductile crust, obtained by removing the sand layer after successful experiments, showed that extension produced a prominent doming of the silicone layers (Figs. 2 and 7). In all models, lateral extension promoted a ductile flow of the silicone which was vertically flattened and laterally extruded towards the dome cores, resulting in the thinning of the ductile crust away from the domes and thickening at the cores (see for instance the $1/\beta$ factor in Fig. 8). Typically, uprising of the lower crust occurred in the central part of the models corresponding to the area of major extension; in plan view, ductile domes were characterised by an elongated shape, with the main axis oblique to the central VD (Figs. 2 and 7). En-echelon

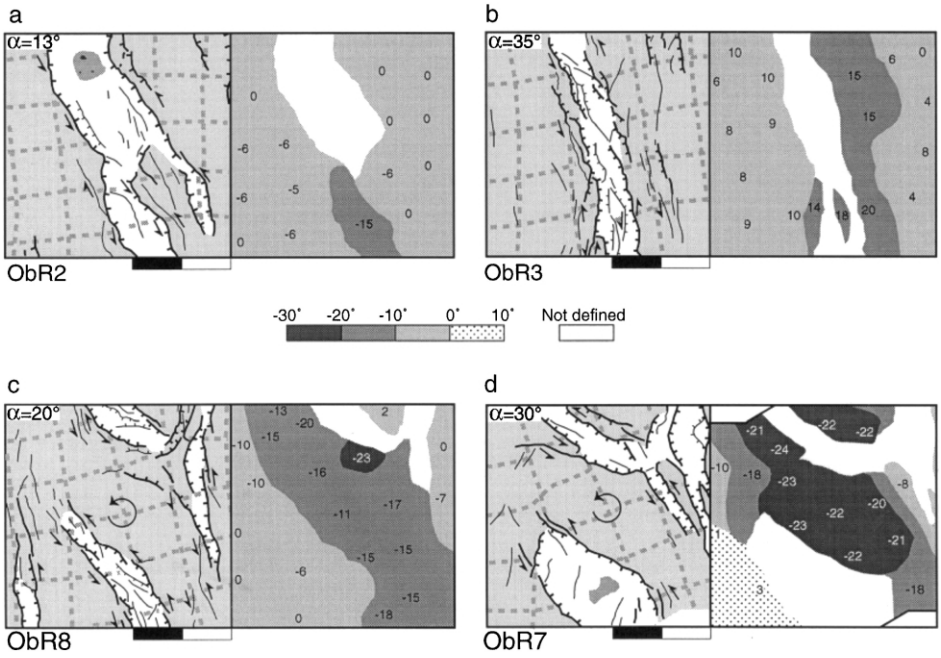

Fig. 5. Measure of block rotation inside models with magma (a and b) and without magma at depth (c and d). Counter clockwise rotations are indicated with negative values while clockwise rotations are indicated with positive angles. The scale bars are in cm.

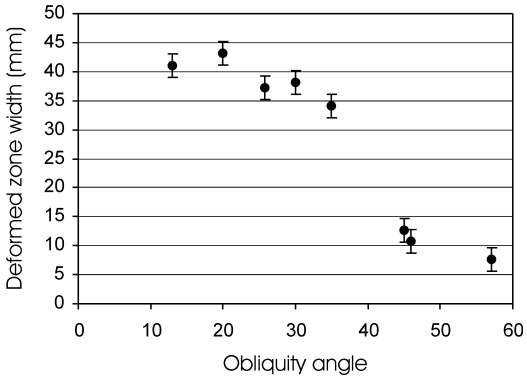

Fig. 6. Deformed zone width plotted against the obliquity angle (α). Please note the abrupt decrease in values of the deformed zone with for obliquity angles of 35–45°.

pattern of domes were also observed in models with $\alpha \leqslant 35°$, though the most developed dome always formed below the main central graben (Fig. 7a–c). Minor external domes orthogonal to the direction of extension formed below major normal faults (Fig. 7a and b).

In orthogonal rifting models, two major domes parallel to the central VD formed beside the boundaries of the initial magma layer (e.g. Model ObR9; Fig. 2a).

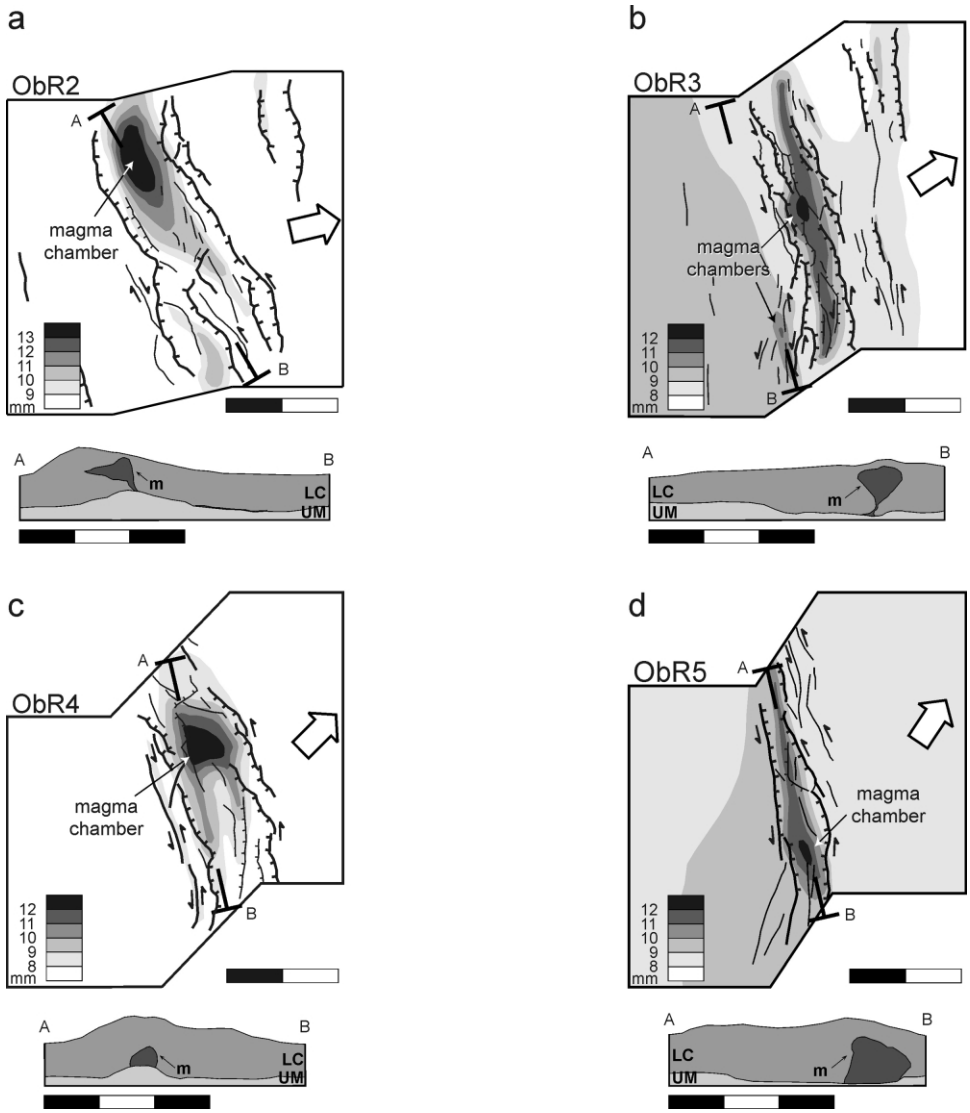

Fig. 7. Cutting of transversal and longitudinal sections has allowed the determination of the 3D internal structure of the models. In all models the 3D structure reveals the occurrence of a marked uplifted top of the lower crust below the graben axis. The location of magma emplacement is indicated.

3.4. Magma emplacement

During the experiments, the underplated magma typically emplaced at the core of lower crust domes, defining an oblique trend to the VD as well as to the initial magma reservoir (Figs. 2c–f and 7). The presence of magma generated a dome amplification, which, for high obliquity model (ObR5), resulted in a major thickening of the domes' core ($1/\beta > 1$; Fig. 8).

Intrusions in the lower crust were associated with major shear zones (Figs. 2 and 7), giving rise to magma bodies characterised by an high length/width ratio, with values up to 6 (e.g. model

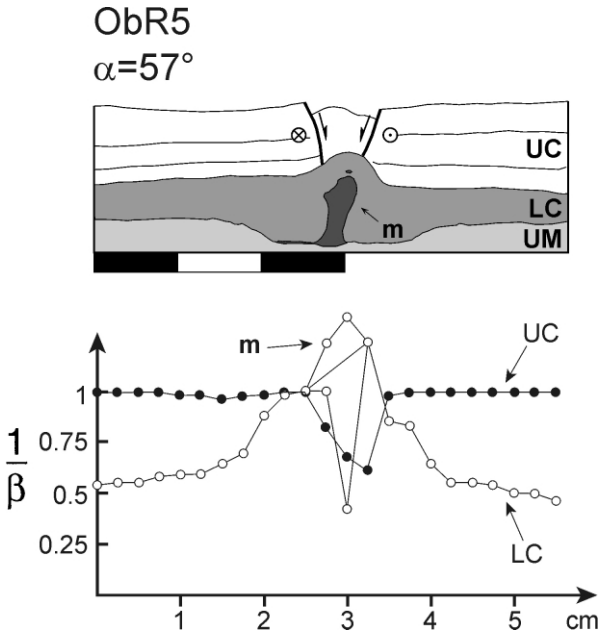

Fig. 8. $1/\beta$ values across model ObR5. Note the absolute thickening of the lower crust below the central graben as denoted by $1/\beta > 1$. Dashed line represents thickness of both lower crust and magma. The scale bars are in cm.

ObR5; compare sections in Fig. 2f with the corresponding sections in Fig. 7d). In models ObR3 and ObR4 part of the magma initially underplated below the Moho reached the surface defining elliptical areas that followed the oblique trend of the upper crust faults (Fig. 2d). In model ObR3, an en-echelon pattern of magmatic chambers is defined by the extruded magma and by another magma body emplaced within a lower crust dome (Figs. 2d and 7b).

During orthogonal rifting, magma emplacement occurred in the ductile domes which formed beside the initial magma reservoir, with a pattern that was parallel to the central VD (and orthogonal to the stretching vector) (Fig. 2a).

4. Discussion

4.1. Summary of results

Experiments presented in this paper invariably showed a deformation pattern reflecting the main features that characterise oblique rifting (e.g. Tron and Brun, 1991): (1) en-echelon fault patterns, (2) mean fault trends oblique to the extension vector, (3) strain partitioning between different sets of faults, and (4) fault dips generally steeper than in pure dip-slip normal faults. Deformation notably started with the development of en-echelon faults that typically joined together giving rise to major grabens in the central area of the models. The border faults of these grabens generally showed tortuous fault traces, characteristic of segmented fault systems (e.g. Clifton et al., 2000).

Experimental results indicate that two important parameters control the surface fault pattern: (1) the angle of obliquity (α), and (2) the presence of magma underplated at the base of the crust.

The obliquity angle (α) controls the ratio between the shearing and the orthogonal stretching components of deformation and hence the structural pattern of the models (e.g. Withjack and Jamison, 1986; Tron and Brun, 1991; Clifton et al., 2000). For $\alpha \leqslant 35^\circ$, deformation is diffused over a wide region as it is partitioned between oblique-slip faults in the central area above the VD and dip-slip normal faults outside this area (Fig. 2c, d and e; Fig. 4). Dip-slip faults are parallel to the VD while oblique-slip faults are oblique to both the VD and the extension vector (Fig. 4). On the contrary, for $\alpha \geqslant 45^\circ$, deformation is more concentrated and no normal faults are observed outside the area above the central VD (Fig. 2e, f and h). Narrow grabens develop in the central region of the model and the extensional strain is partitioned between normal to oblique-slip bounding faults and external strike-slip faults (Fig. 2e, f and h). Both sets of faults are oblique to the VD and to the stretching vector (Fig. 4).

The major change in surface fault pattern (and hence in strain partitioning) occurs for obliquity angles in the range of 35–45°, where also an abrupt decrease in the width of the deformed zone is observed (Fig. 6). These transitional angles are similar to those observed in sand-modelling by Tron and Brun (1991), but they are lower than the values of about 45–60° observed in clay-models by Withjack and Jamison (1986) and Clifton et al. (2000). In agreement with Tron and Brun (1991), our results support the hypothesis that this difference is due to the intrinsic properties of the two different materials used in the experiments. However, model results, and in particular the width of deformed zone, are also dependent on the applied strain rate which controls the coupling between brittle and ductile crust (e.g. Allemand et al., 1989; Tron and Brun, 1991; Brun and Tron, 1993; Brun, 1999). In our models displacements are applied along the narrow VD and then transferred by viscous coupling at the base of the upper brittle layer: an increase in coupling is expected to decrease the fault spacing and to increase the width of the deformed zone (e.g. Allemand et al., 1989; Tron and Brun, 1991; Brun and Tron, 1993; Brun, 1999).

Influence on fault pattern of magma at depth is illustrated by the comparison of models performed with or without magma. Experimental results suggest that for $\alpha \geqslant 45^\circ$ the presence of magma at depth has a low influence on the structural pattern, with a final fault distribution that is substantially similar in the two types of models (Figs. 2, and 4). On the contrary, for $\alpha \leqslant 35^\circ$ the underplated magma strongly controls the surface fault pattern, leading to a strain localisation above the initial magma reservoir that represents a low strength layer in the central part of the model (Figs. 2–5). The effect of this localisation is that deformation is mostly accommodated by central oblique-slip faults, thus reducing the strain partitioning and partly inhibiting the development of external normal faults.

4.2. Lower crust doming and magma emplacement

Oblique extension has a strong influence on the deformation of the lower crust, as demonstrated by the different patterns of doming observed during experiments with different obliquity (Figs. 7). In particular, lower crust domes form parallel to the central VD in orthogonal rifting models, while during oblique extension they are oblique to both the central VD and the stretching vector, and in some cases are en-echelon arranged (e.g. models ObR2 and 3; Fig. 7a and b). Crustal domes are characteristically developed below major grabens in the upper crust, with the

surface morphology that typically is the inversion of the morphology of the ductile lower crust top (e.g. Dauteuil and Mart, 1998; Mart and Dauteuil, 2000; see also Fig. 8).

We interpret this process of doming in the lower crust as a typical response of viscous fluids to stretching of the continental crust. In this process, the upwelling can be view as a space-filling reaction to the lateral shifting of major crustal blocks, in a similar fashion to the "reactive diapirism" model by Jackson and Vendeville (1994), though our analog lower crust was denser that the overlying brittle crust.

Experimental results indicate that there is an interplay between deformation and the presence of an underplated magma during oblique rifting: (1) the occurrence of magma at depth localises strain in the overlying crust, thus controlling the surface fault pattern (see Section 4.1), whereas (2) deformation causes magma to emplace within the lower crust domes with an oblique, and some cases, en-echelon pattern. In the case of ductile doming, models suggest that magma emplacement occurs as passive response to the doming process: domes, indeed, developed even when magma was not placed at the base of the crust (e.g. ObR.6-8, Fig. 2g and h). Nevertheless, although magma uprising does not play an active role in the doming process, when magma buoyancy is involved the domes development is enhanced (e.g Lister and Baldwin, 1993), leading in some cases to an absolute thickening of the lower crust (Fig. 8). This behaviour is probably favoured by the low strain rate imposed to the models and the correspondent brittle/ductile decoupling that promotes a convergent lateral flow in the ductile crust of dome regions.

The main difference in the pattern of magma emplacement occurred between oblique and orthogonal rifting models. In orthogonal rifting model (ObR9; Fig. 2a), magma underplating the base of the crust was laterally squeezed toward the cores of lower crust domes (e.g. Bonini et al., in press). In this case, major magma accumulation occurs in the footwall of major normal faults, in a mechanism which is similar to the extensional footwall growth by Quirk et al. (1998). Thus, magma intrusions are expected to occur on the shoulders of rift valleys, with a rift-parallel trend which is also parallel to the initial magma reservoir (Bonini et al., in press). Such a mechanism may account for the magmatic and volcanic activity which is often observed in the footwall of major normal faults in extensional settings, such as narrow rifts (Bonini et al., in press) and core complexes (Schermer and Gans, 1985; Hauser et al., 1987; King and Ellis, 1990; Ellis and King, 1991; Lister and Baldwin, 1993; Parsons and Thompson, 1993).

During oblique rifting, the combination of shearing and doming in the lower crust favoured an oblique, and in some cases en-echelon, magma emplacement pattern (e.g. model ObR3), which occurred above the initial magma reservoir and within the main rift zone (Figs. 2, 7 and 9). Shear zones in the lower crust, that accommodate the strike-slip component of displacement, exerted a major control on magma emplacement, that resulted in sheeted intrusions with high length/width ratio. Similarly, oblique faults in the upper crust controlled the extrusion of magma up to the surface serving as conduits for ascending magmas. Our models, showing magma emplacement occurring in oblique or en-echelon lower crust domes, correlate well with natural examples reported from both continental and oceanic rifts, as described in the following sections.

4.3. Comparison with nature

Previous analogue model results have been compared to natural examples in extensional settings on the basis of similarities in the surface fault pattern, mainly resulting from a statistical

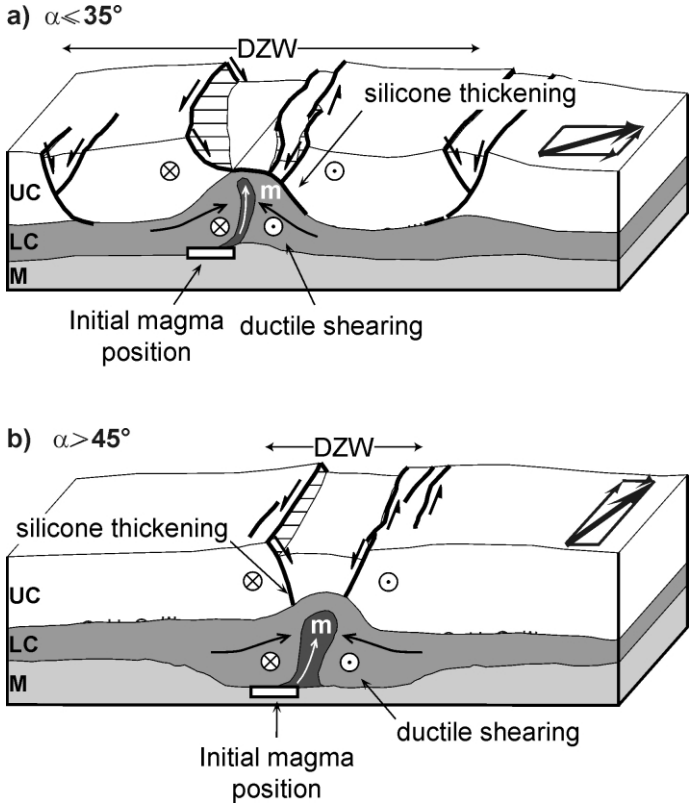

Fig. 9. Schematic diagrams showing the mechanism of domes' formation and magma emplacement observed in the centrifuge models for low (a) and high (b) obliquity rifting. LC: lower crust; M: mantle; m: magma; DZW: deformed zone width. Arrows schematically indicate the ductile lateral flow trajectories inferred for the lower crust and underplated magma. See text for further explanations.

analysis of fault directions (Withjack and Jamison, 1986; Tron and Brun, 1991; Dauteuil and Brun, 1993; McClay and White, 1995; Bonini et al., 1997; Mart and Dauteuil, 2000; Clifton et al., 2000). In particular, these works have demonstrated the applicability of analogue model results to a wide range of extensional areas, such as the Gulf of California, the Gulf of Aden, the East African Rift System, the Red Sea, the North Sea, the Rhine Graben and even the oceanic rifts.

The comparison of our results with natural examples has to take into account both (1) the observed structural pattern and (2) the resulting distribution of magma bodies oblique to the main rift axis and to the assumed location of the initial magma reservoir. Examples from both continental rifts and oceanic ridges are reported below.

4.3.1. Main Ethiopian Rift

One of the best examples of magmatic and fault belts oblique to the rift trend is found in the Main Ethiopian Rift (MER; Fig. 10a), where, according to Bonini et al. (1997) and Boccaletti et al. (1998), a first phase of orthogonal rifting was followed by a second phase characterised by a stretching vector oblique (of about 50°) to the rift trend (Fig. 10a). This kinematics resulted in a strong sinistral component of movement along the rift structure, that was accommodated by the

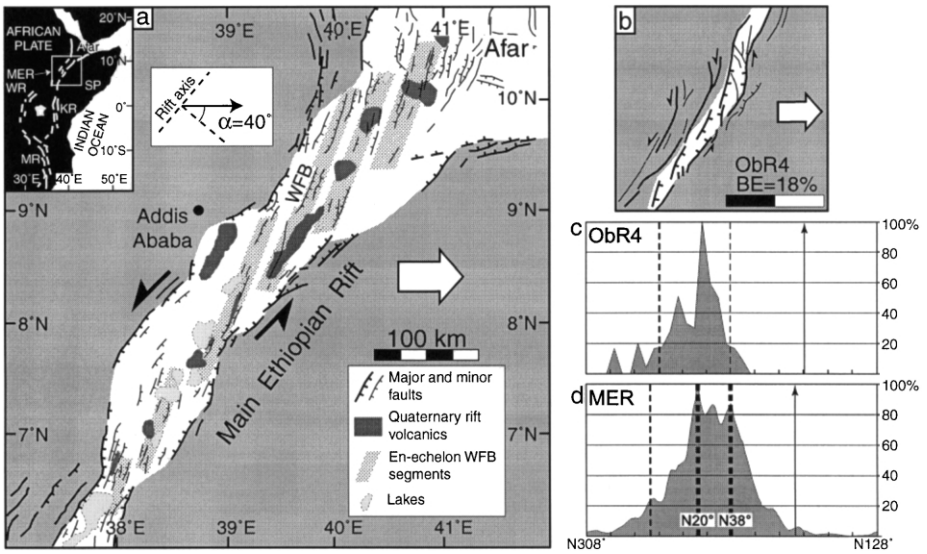

Fig. 10. Comparison of model results with the oblique faulting and volcanism in the Main Ethiopian Rift (MER). Inset shows the location of the MER; KR: Kenya Rift, MR: Malawi Rift, SP: Somalian Plate, WR: Western Rift. (a) Schematic structural map of the MER (after Hayward and Ebinger, 1996 and Boccaletti et al., 1999). Please note the coincidence of Quaternary rift volcanics with the en-echelon fault system of the WFB; (b) top-view line drawing of model ObR4 for $\beta = 1.20$, which corresponds to value observed in the MER (Ebinger et al., 1993); (c) histogram of fault distribution for model ObR4 and correspondent histogram (d) for the MER (after Bonini et al., 1997). Please note the coincidence between the peak related to the oblique faults of the WFB (N20° in d) and the main peak in model ObR4 (in c). See text for further explanations.

development of the Wonji Fault Belt (WFB; Mohr, 1962, 1967, 1987), a system composed of N–S to N20°E trending en-echelon right-stepping faults, which are oblique (of about 20°) to the N30°E–N40°E trending border faults (Fig. 10a). The WFB, which started to form around 1.8–1.6 Ma ago (Meyer et al., 1975), controlled the eruption of basaltic lavas as evidenced by the alignments of spatter cones and the trend of eruptive fractures (Mohr, 1967; Boccaletti et al., 1998, 1999; Mazzarini et al., 1999).

The structural pattern and the distribution of the volcanism in the MER match the results of analogue experiments presented in the previous sections. In particular the models are able to describe the second phase of rift evolution, characterised by oblique extension and the consequent concentration of the deformation inside the MER. This structural setting developed newly formed en-echelon strike-slip faults that accommodated the sinistral component of the slip motion (Bonini et al., 1997). In this structural frame, the magma, which is assumed to underplate the continental crust, is uprising to form crustal magma bodies feeding unimodal central volcanoes obliquely arranged with respect to the main rift trend (Mazzarini et al., 1999), as illustrated by analogue experiments. The similarity between nature and experiments is further supported by the resemblance of fault distribution, as the main peak in the histogram of fault orientation of the MER, related to the WFB oblique faulting (N20° in Fig. 10d), displays the same orientation as main peak of fault distribution in model ObR4 (Fig. 10c). However, no correspondence has been observed for rift-parallel faults peak in the MER (N38° in Fig. 10d). This discrepancy is interpreted as a consequence of

the two-phase evolution of the MER that produced early normal faults linked to orthogonal extension, whereas oblique faulting was generated during the second phase of oblique extension.

4.4. Oceanic ridges

Other examples of oblique rifting controlling magmatic and volcanic patterns are described for some oceanic ridges, such as the Reykjanes Ridge (RR), south of Iceland, and the Mohns Ridge (MR), in the Norwegian-Greenland Sea (e.g. Searle and Laughton, 1981; Dauteuil and Brun, 1993, 1996; Parson et al., 1993; Appelgate and Shor, 1994; McAllister et al., 1995; Fig. 11). In these low spreading ridges, a first phase of orthogonal spreading resulted in the development of axial valleys representing the surface expression of a deformable band of oceanic lithosphere (e.g. Dauteuil and Brun, 1993, 1996). A reorientation of the stress field determined the spreading vector to be oblique (of about 30–40°) to this deformable band, giving rise to a deformation pattern

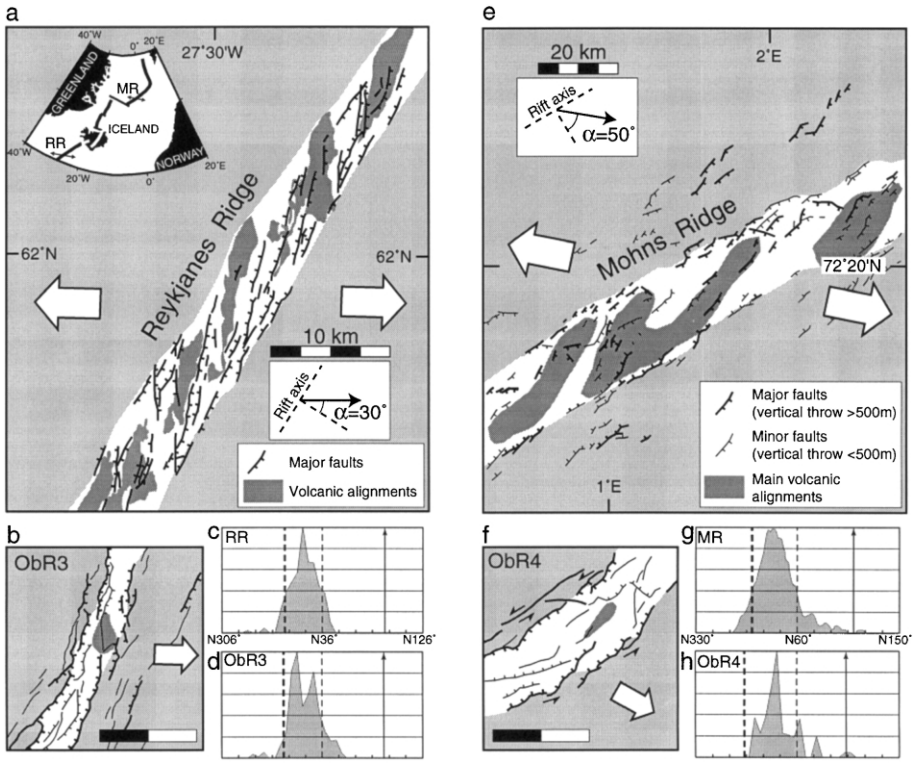

Fig. 11. Comparison of model results with the fault and volcanic patterns in the Reykjanes and Mohns Ridges (RR and MR, respectively). Inset shows the location of the MR and RR in the North Atlantic Ocean; thick lines represent the Mid Atlantic Ridge, whereas lines with arrows indicate the spreading direction. (a) Structural pattern in the RR (after Murton and Parson, 1993). Note the oblique en-echelon arrangement of the volcanic alignments; (b) final top view line drawing of model ObR3; (c) histogram of fault distribution for model ObR3 and correspondent histogram (d) for the RR; (e) structural pattern in the MR (after Dauteuil and Brun, 1996); (f) top view line drawing of model ObR4; (g) histogram of fault distribution for model ObR4 and correspondent histogram (h) for the MR. Please note the coincidence between major and minor peaks in the histograms of models (c and g) and the two natural examples (d and h).

characterised by en-echelon faults oblique to the axial valley trend (Fig. 11a and e). Typically, this structural pattern is accompanied by the development of en-echelon volcanic alignments (e.g. Murton and Parson, 1993; Appelgate and Shor, 1994). Volcanoes are indeed preferentially located along oblique structures, with fault zones controlling the upward migration of magmas (e.g. Dauteuil and Brun, 1996; Tuckwell et al., 1998; Fig. 11a and e).

Although the oceanic crust shows different brittle/ductile ratio and thickness with respect to the modelled continental crust, our experimental results show a good correlation with the structural and volcanic pattern observed in these oceanic ridges (e.g. Dauteuil and Brun, 1993; Fig. 11). This is documented by the similar orientation of the main peak in the histograms of fault distribution corresponding to structures oblique to the stretching vector and to the axial valley trend (Fig. 11c–d and g–h). Both in nature and experiments, minor peaks in the fault distribution curve correspond to rift-parallel faults (Fig. 11c–d and g–h).

5. Conclusions

The current series of scaled centrifuge models have investigated the deformation produced by oblique extension considering different angles of obliquity (from 0° to about 60°) and the presence of a magma initially underplated at the base of the crust. Experiments have mainly investigated the dynamic relationships between deformation and magma emplacement. The main conclusions of our modelling are the following:

1. The structural pattern is invariably characterised by the presence of en-echelon faults, with mean trends not perpendicular to the stretching vector and a component of movement varying from pure normal to strike-slip. Typically the deformation is partitioned between these different sets of structures, thus reproducing the main characteristics of oblique rifting.
2. The angle of obliquity (α), controlling the ratio between the shearing and stretching component of movement, strongly affects the deformation pattern of models. For $\alpha \leqslant 35^\circ$, a strain partitioning arises between oblique-slip and normal faults, whereas for $\alpha \geqslant 45^\circ$ the deformation is more concentrated and partitioned between oblique-slip and strike-slip faults.
3. The presence of magma has a strong influence on the surface fault pattern the for $\alpha \leqslant 35^\circ$ resulting in a strain localisation and a reduced strain partitioning. When magma is absent, the deformation is diffused over the whole model surface and the fault pattern is more complex.
4. Magma intrusions, following the trend of lower crust domes, typically occur obliquely to the initial magma reservoir and in some cases with an en-echelon arrangement. Magma bodies are normally located within the ductile domes, approximately above the initial magma chamber. For $\alpha \geqslant 45^\circ$, shear zones affects the ductile domes giving rise to sheeted intrusions with high length/width ratio.
5. Points 3 and 4 suggest that there is a dynamic interplay between deformation and the occurrence of underplated magma during oblique rifting.
6. Model results are comparable with natural examples of continental rifts (Main Ethiopian Rift) and oceanic ridges (Reykjanes and Mohns Ridges), showing en-echelon volcanic and fault belts oblique to the main rift axis (and to the assumed trend of the underplated magma).

References

Allemand, P., Brun, J.P., Davy, P., Van Den Driessche, J., 1989. Symétrie et asymétrie des rifts et mécanismes d'amincissement de la lithospère. Bull. Soc. Géol. Fr. 8, 445–451.

Appelgate, B., Shor, A.N., 1994. The northern mid-Atlantic and Reykjanes Ridges: spreading centre morphology between 55°50′N and 63°00′N. Journal of Geophysical Research 99, 17935–17956.

Arzi, A.A., 1978. Critical phenomena in the rheology of partially melted rocks. Tectonophysics 44, 173–184.

Bergantz, G.W., 1989. Underplating and partial melting: implications for melt generation and extraction. Science 245, 1093–1095.

Boccaletti, M., Bonini, M., Mazzuoli, R., Abebe, B., Piccardi, L., Tortorici, L., 1998. Quaternary oblique extensional tectonics in the Ethiopian Rift (Horn of Africa). Tectonophysics 287, 97–116.

Boccaletti, M., Bonini, M., Mazzuoli, R., Trua, T., 1999. Pliocene–Quaternary volcanism and faulting in the northern Main Ethiopian Rift (with two geological maps at scale 1:50,000). Acta Vulcanologica 11, 83–97.

Bonini, M., Sokoutis, D., Mulugeta, G., Boccaletti, M., Corti, G., Innocenti, F., Manetti, P., Mazzarini, F., Dynamics of magma emplacement in centrifuge models of continental extension with implications for flank volcanism. Tectonics (in press).

Bonini, M., Souriot, T., Boccaletti, M., Brun, J.P., 1997. Successive orthogonal and oblique extension episodes in a rift zone: laboratory experiments with application to the Ethiopian Rift. Tectonics 16, 347–362.

Brun, J.-P., 1999. Narrow rifts versus wide rifts: inferences for the mechanics of rifting from laboratory experiments. Phil. Trans. Roy. Soc. Lond. A 357, 695–712.

Brun, J.-P., Tron, V., 1993. Development of the North Viking Graben: inferences from laboratory modelling. Sedimentary Geology 86, 31–51.

Buck, W.R., 1991. Modes of continental lithospheric extension. Journal of Geophysical Research 96, 20161–20178.

Chèry, J., Daignières, M., Lucazeau, F., Vilotte, J.-P., 1989. Strain localization in rift zones (case of a thermally softened lithosphere): a finite element approach. Bulletin de la Societé Géologique de France 3, 437–443.

Clifton, A.E., Schlische, R.W., Withjack, M.O., Ackermann, R.V., 2000. Influence of rift obliquity on fault-population systematics: results of experimental clay models. Journal of Structural Geology 22, 1491–1509.

Dauteuil, O., Brun, J.P., 1993. Oblique rifting in a low spreading ridge. Nature 361, 145–148.

Dauteuil, O., Brun, J.P., 1996. Deformation partitioning in a slow spreading ridge undergoing oblique extension: Mohns Ridge, Norwegian Sea. Tectonics 15, 870–884.

Dauteuil, O., Mart, Y., 1998. Analogue modelling of faulting pattern, ductile deformation, and vertical motion in strike-slip fault zones. Tectonics 17, 303–310.

Ebinger, C.J., Yemane, T., WoldeGabriel, G., Aronson, J.L., Walter, R.C., 1993. Late Eocene—recent volcanism and faulting in the southern main Ethiopian Rift. Journal of the Geological Society London 150, 99–108.

Ellis, M., King, G., 1991. Structural control of flank volcanism in continental rifts. Science 254, 839–842.

Fadaie, K., Ranalli, G., 1990. Rheology of the lithosphere in the East African Rift System. Geophysical Journal International 102, 445–453.

Furlong, K.P., Fountain, D.M., 1986. Continental crustal underplating: thermal considerations and seismic-petrologic consequences. Journal of Geophysical Research 91, 8285–8294.

Fyfe, W.S., 1992. Magma underplating of continental crust. Journal of Volcanology and Geothermal Research 50, 33–40.

Hauser, E., Potter, C., Hauge, T., Burgess, S., Burtch, S., Mutschler, J., Allmendinger, R., Brown, L., Kaufman, S., Olivier, J., 1987. Crustal structure of eastern Nevada from COCORP deep seismic reflection data. Geological Society of America Bullettin 99, 833–844.

Hayward, N.J., Ebinger, C.J., 1996. Variations in the along-axis segmentation of the Afar Rift system. Tectonics 15, 244–257.

Hubbert, M.K., 1937. Theory of scaled models as applied to the study of geological structures. Geological Society of America Bulletin 48, 1459–1520.

Jackson, M.P.A., Vendeville, B., 1994. Regional extension as a geologic trigger for diapirism. Geological Society of America Bullettin 106, 57–73.

King, G., Ellis, M., 1990. The origin of large local uplift in extensional regions. Nature 348, 689–693.

Lister, G.S., Baldwin, S.L., 1993. Plutonism and the origin of metamorphic core complexes. Geology 21, 607–610.

Mart, Y., Dauteuil, O., 2000. Analogue experiments of propagation of oblique rifts. Tectonophysics 316, 121–132.
Mazzarini, F., Abebe, T., Innocenti, F., Manetti, P., Pareschi, M.T., 1999. Geology of the Debre Zeyt area (Ethiopia) (with a geological map at scale 1:100.000). Acta Vulcanologica 11, 131–141.
McAllister, E.J., Cann, J., Spencer, S., 1995. The evolution of crustal deformation in an oceanic extensional environment. Journal of Structural Geology 17, 183–199.
McClay, K.R., White, M.J., 1995. Analogue modelling of orthogonal and oblique rifting. Marine and Petroleum Geology 12, 137–151.
McKenzie, D.P., Jackson, J.A., 1983. The relationships between strain rates, crustal thickening, paleomagnetism, finite strain and fault movements within a deforming zone. Earth and Planetary Science Letters 65, 185–202.
McKenzie, D.P., Jackson, J.A., 1986. A block model of distributed deformation by faulting. Journal of the Geological Society London 143, 349–353.
Merle, O., Abidi, N., 1995. Approche experimentale du functionnement des rampes emergentes. Bulletin de la Societé Géologique de France 166, 439–450.
Merle, O., Vendeville, B., 1995. Experimental modelling of thin-skinned shortening around magmatic intrusions. Bullettin of Volcanology 57, 33–43.
Meyer, W., Pilger, A., Rosler, A., Stets, J., 1975. Tectonics evolution of the noerhtern part of the Main Ethiopian Rift in Southern Ethiopia. In: Pilger, A., Rosler, A. (Eds.), Afar Depression of Ethiopia Vol. 14. IUCG Sci. Rep, Stuttgart, pp. 352–362.
Mohr, P., 1962. The Ethiopian Rift System. Bulletin of the Geophysical Observatory of Addis Ababa 5, 33–62.
Mohr, P., 1967. The Ethiopian Rift System. Bulletin of the Geophysical Observatory of Addis Ababa 11, 1–65.
Mohr, P., 1987. Patterns of faulting in the Ethiopian Rift Valley. Tectonophysics 143, 169–179.
Morley, C.K., 1999a. How successful are analogue models in addressing the influence of pre-existing fabrics on rift structures? Journal of Structural Geology 21, 1267–1274.
Morley, C.K., 19999b. Tectonics evolution of the East African Rift System and the modifying influence of magmatism: a review. Acta Vulcanologica 11, 1–19.
Mulugeta, G., 1988. Squeeze-box in the centrifuge. Tectonophysics 148, 323–335.
Murton, B.J., Parson, L.M., 1993. Segmentation, volcanism and deformation of oblique spreading centers—a quantitative study of the Reykjanes Ridge. Tectonophysics 222, 237–257.
Parson, L.M. et al., 1993. En echelon axial volcanic ridges at the Reykjanes Ridge: a life cycle of volcanism and tectonics. Earth and Planetary Science Letters 117, 73–87.
Parsons, T., Sleep, N.H., Thompson, G.A., 1992. Host rock rheology controls on the emplacement of tabular intrusions: implications for underplating of extending crust. Tectonics 11, 1348–1356.
Parsons, T., Thompson, G.A., 1993. Does magmatism influence low-angle normal faulting? Geology 21, 247–250.
Quirk, D.G., D'Lemos, R.S., Mulligan, S., Rabti, M.R., 1998. Insights into the collection and emplacement of granitic magma based on 3D seismic images of normal fault-related salt structures. Terra Nova 10, 268–273.
Ramberg, H., 1981. Gravity, Deformation and the Earth's Crust. Academic Press, London.
Schermer, E.R., Gans, P.B., 1985. Isotope and trace-elements geochemistry of syn-extensional volcanic rocks, east-central Nevada. EOS Trans. AGU 66, 1138.
Scott, S.D., Benes, V., 1996. Oblique rifting in the Havre Trough and its propagation into the continental margin of New Zealand: comparison with analogue experiments. Marine Geophysical Researches 18, 189–201.
Searle, R.C., Laughton, A.S., 1981. Fine-scale sonar study of tectonics and volcanism on the Reykjanes ridge. Oceanol. Acta 4, 5–13.
Tuckwell, G.W., Bull, J.M., Sanderson, D.J., 1998. Numerical models of faulting of oblique spreading centers. Journal of Geophysical Research 103, 15473–15482.
Tron, V., Brun, J.-P., 1991. Experiments on oblique rifting in brittle-ductile systems. Tectonophysics 188, 71–84.
Withjack, M.O., Jamison, W.R., 1986. Deformation produced by oblique rifting. Tectonophysics 126, 99–124.
Weijermars, R., 1997. Principles of Rock Mechanics. Alboran Science Publishing, Amsterdam.